

ARTICLE

OPEN



Nondestructive identification of softness via bioinspired multisensory electronic skins integrated on a robotic hand

Ye Qiu^{1,2,3}, Shenshen Sun^{1,2,3}, Xueer Wang⁴, Kuanqiang Shi^{1,2,3}, Zhiqiang Wang^{1,2,3}, Xiaolong Ma^{1,2,3}, Wenan Zhang⁴, Guanjun Bao^{1,2,3}, Ye Tian^{1,2,3}, Zheng Zhang^{1,2,3}, Hao Ding^{1,2,3}, Hao Chai⁵, Aiping Liu⁶ and Huaping Wu^{1,2,3}✉

Tactile sensing is essentially required for dexterous manipulation in robotic applications. Mimicking human perception of softness identification in a non-invasive fashion, thus achieving satisfactory interaction with fragile objects remains a grand challenge. Here, a scatheless measuring methodology based on the multisensory electronic skins to quantify the elastic coefficient of soft materials is reported. This recognition approach lies in the preliminary classification of softness by piezoelectric signals with a modified machine learning algorithm, contributing to an appropriate contact force assignment for subsequent quantitative measurements via strain sensing feedback. The integration of multifunctional sensing system allows the manipulator to hold capabilities of self-sensing and adaptive grasping motility in response to objects with the various softness (i.e., kPa-MPa). As a proof-of-concept demonstration, the biomimetic manipulator cooperates with the robotic arm to realize the intelligent sorting of oranges varying in freshness, paving the way for the development of microsurgery robots, human-machine interfacing, and advanced prosthetics.

npj Flexible Electronics (2022)6:45; <https://doi.org/10.1038/s41528-022-00181-9>

INTRODUCTION

The primary sensory organ of the human body, the skin, enables the cooperation of the mechanoreceptors and neurons to perceive tactile stimuli and mediate daily interactions with the surrounding environment^{1–3}. The emulation of human sensation, neuronal transmission, and adaptive motility is an inspiring and challenging research topic to develop intelligent robotics in the emerging fields of human-machine interfacing and advanced prosthetics^{4–15}. The development of adaptive interaction in a robotic body requires design strategies that can provide sufficient sensing feedback to control motion and connect the robot with the surrounding environment^{16–28}. Understanding in biology and advances in electronic technologies has paved the way for creating intelligent soft robots with perception feedback and stimulus-responsive motility^{29–42}.

Enormous demand and promising prospects for bioinspired intelligent robotics have led to notable progress in object identification^{43–45}. Although visual recognition methods have evolved to recognize shape features and realize texture determination effectively, they struggle to detect internal softness features and thus expose limitations in applications of minimally invasive surgery, industrial picking, and prosthetic rehabilitation. In contrast, flexible sensors-based tactile perception technologies have unique advantages in assisting intelligent robots to achieve recognition of tissue, fine motor tasks, and interactive awareness^{46–51}. With the aid of materials and designs of micro/nanostructures that are sensitive to physical stimuli, flexible sensors with various sensing mechanisms (e.g., piezoelectric^{52,53}, magnetic⁵⁴, and piezoresistive^{55,56}) have emerged to realize softness recognition of touched objects. Nevertheless, these measuring strategies based on a single sensing mechanism are susceptible to interference from environmental factors such as

nonlinear friction and electrical disturbances, and therefore have limited perception and measurement accuracy.

To address these restrictions, additional efforts on softness recognition have been exploited in multiple sensory feedback of tactile information that rely on the integration of multifunctional sensing schemes to achieve precise object discrimination^{57–59}. For instance, a bioinspired stretchable membrane-based sensor that consists of capacitive and strain sensors has been proposed to recognize compliance of touched materials using pressure and strain-sensing mechanoreceptors⁵⁷. The development of multisensory perception in one compact system has achieved the identification of softness properties, their sensing mechanisms depend on the relationship between force (stress) and deformation (strain) determined by the contact area and indentation depth of the measuring objects. Despite the above progress, however, these identifying methods still require deformation feedback and usually suffer from the problem of permanent damage when applying unprejudiced contact force to a sample regardless of fragility, which strictly limits the application of these systems for future health monitoring, soft robotics, and wearable devices. Thus, it is highly desirable to develop and demonstrate a multifunctional sensing system with multiple feedback capabilities to realize softness recognition in a non-invasive manner, especially for the grasping task of delicate and vulnerable objects in intelligent robots and human-machine interfaces.

Here, we propose a non-invasive measurement for softness quantification of soft materials via a bioinspired multifunctional sensing system with the integration of piezoelectric and strain sensing modules. It is enabled through the synergistic effect that includes the preliminary softness classification measured by the piezoelectric layer with machine learning technique, and quantitative elastic coefficient recognition by the strain layer while

¹College of Mechanical Engineering, Zhejiang University of Technology, Hangzhou 310023, China. ²Key Laboratory of Special Purpose Equipment and Advanced Processing Technology, Ministry of Education and Zhejiang Province, Zhejiang University of Technology, Hangzhou 310023, China. ³Collaborative Innovation Center of High-end Laser Manufacturing Equipment (National “2011 Plan”), Zhejiang University of Technology, Hangzhou, China. ⁴College of Information Engineering, Zhejiang University of Technology, Hangzhou 310023, China. ⁵Zhejiang College of Zhejiang University of Technology, Shaoxing 312030, China. ⁶Center for Optoelectronics Materials and Devices, Zhejiang Sci-Tech University, Hangzhou 310018, China. ✉email: wuhuaping@gmail.com

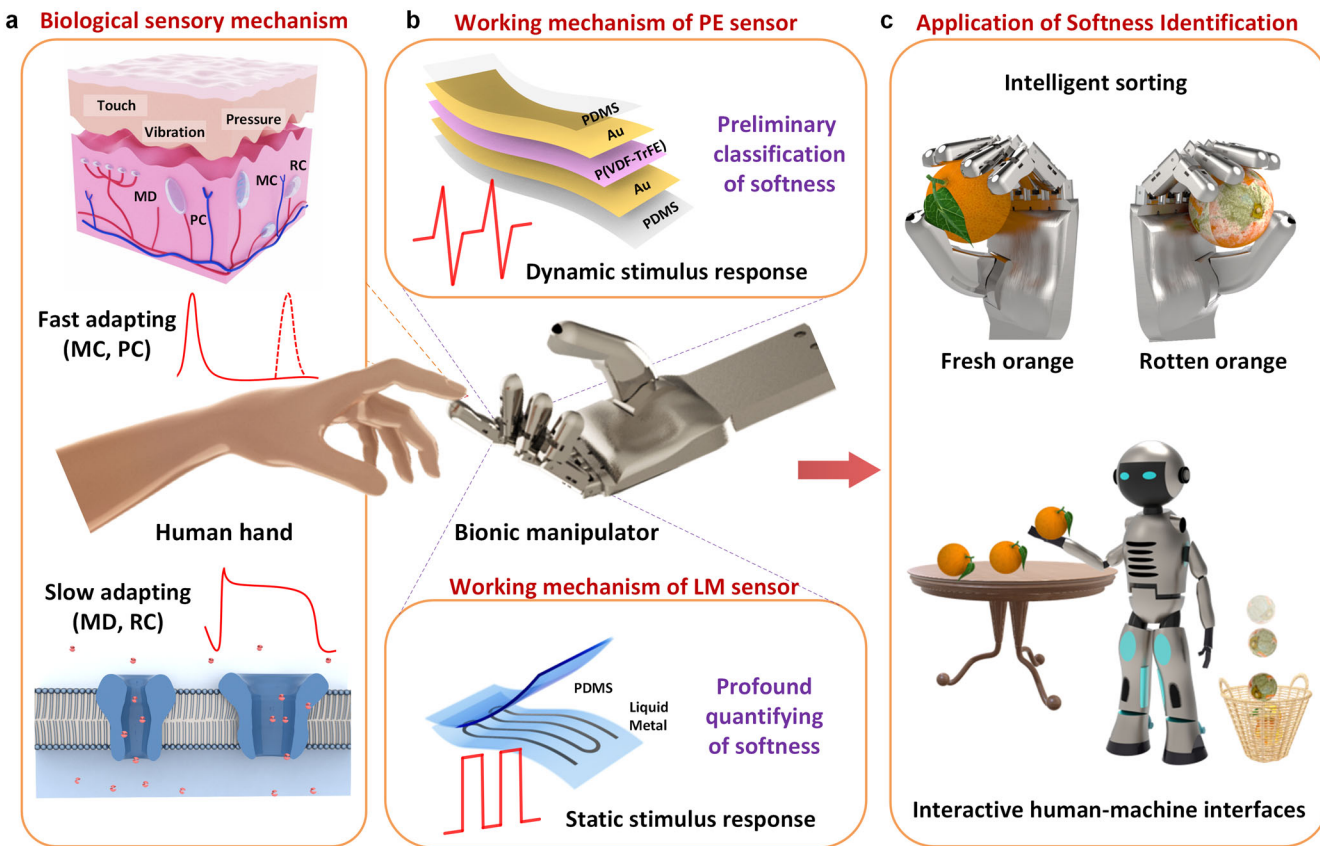


Fig. 1 Human skin-inspired multisensory electronic skins. **a** Schematics illustrations the structure and function of a biological somatosensory system. Human skin consists of fast-adapting mechanoreceptors [Meissner (MC) and Pacinian corpuscles (PC)] for dynamic stimuli, slow-adapting mechanoreceptors [Merkel disc (MD) and Ruffini endings (RE)] for static stimuli. All mechanoreceptors produce receptor potential through ion channels; **b** The biomimetic multisensory electronic skin utilizes the synergistic effect of flexible piezoelectric and piezoresistive modes for softness recognition: the piezoelectric layer mimics the fast-adapting mechanoreceptors (i.e., MC and PC) to detect the dynamic touch for preliminary softness classification. The piezoresistive layer emulates the static stimuli response of slow-adapting mechanoreceptors (i.e., MD and RE) to quantitatively measure the softness; **c** Biomimetic manipulator integrated with multisensory tactile sensors for intelligent sorting.

applying the appropriate contact force based on the classification. The biomimetic manipulator assisted with multimodal sensory feedback is capable of measuring and discriminating the softness of soft materials in real-time, resulting in an effective grasping interaction with vulnerable objects (e.g., tofu and tomato). The integration of the multifunctional sensing system onto a robot arm is demonstrated to realize intelligent sorting, revealing its potential as a promising strategy for soft robotics, human-machine interfaces, and neuroprosthetics.

RESULTS

Design of the multisensory electronic skins

Mechanoreceptors within human skin are responsible for discriminating a variety of mechanical stimuli, including the fast-adapting (FA) receptors (Meissner and Pacinian Corpuscle) that respond to dynamic forces and the slow-adapting (SA) receptors (Merkel Disc and Ruffini Endings) that can detect static pressures^{60–64} (Fig. 1a). The underlying somatosensory mechanism lies in the transmission of ions through the mechanically gated ion channel to generate membrane potential. Inspired by the physiological functions of the human skin, the integrated piezoelectric module in the biomimetic manipulator mimics the perceptive function of the FA receptors to detect high-frequency dynamic stimuli, which can realize a preliminary distinction of softness by the instantaneous pulse signal (Fig. 1b). Meanwhile, the piezoresistive module captures static

stimuli similar to the SA mechanoreceptors, enabling the liquid metal (LM) sensor to maintain the signal from the beginning to the end of pressure and decode the softness profoundly. This synergistic effect demonstrates the promising potential of the multifunctional sensing system for robotic intelligent sorting (Fig. 1c), thus opening up broad application opportunities in neural prosthetics, soft robotics, and interactive human-machine interfaces.

Property characterization of the multisensory sensors

Mimicking the natural intelligence of the human hand in artificial systems with systematical functions of motility and perception, a biomimetic manipulator is designed and 3D printed as the artificial muscle based on the physiological structure and movement of the finger skeleton (Fig. 2a). The overall structure of the index finger consists of the distal, middle, and proximal phalanges, which is connected through bearings, shafts, and torsion springs. The thumb has one degree of freedom and can achieve a side-swinging motion when interacting with objects, which plays the main role in fixing and supporting objects (Supplementary Fig. 1). Such demonstrated functional assembly and control modules (Supplementary Figs. 2 and 3) enable the manipulator can be commanded to grasp various objects with different weights (Supplementary Fig. 4), such as iron needle, screwdriver, pliers, sponge, water bottle, etc. Meanwhile, the biomimetic manipulator heterogeneously integrates the piezoelectric (Polyvinylidene

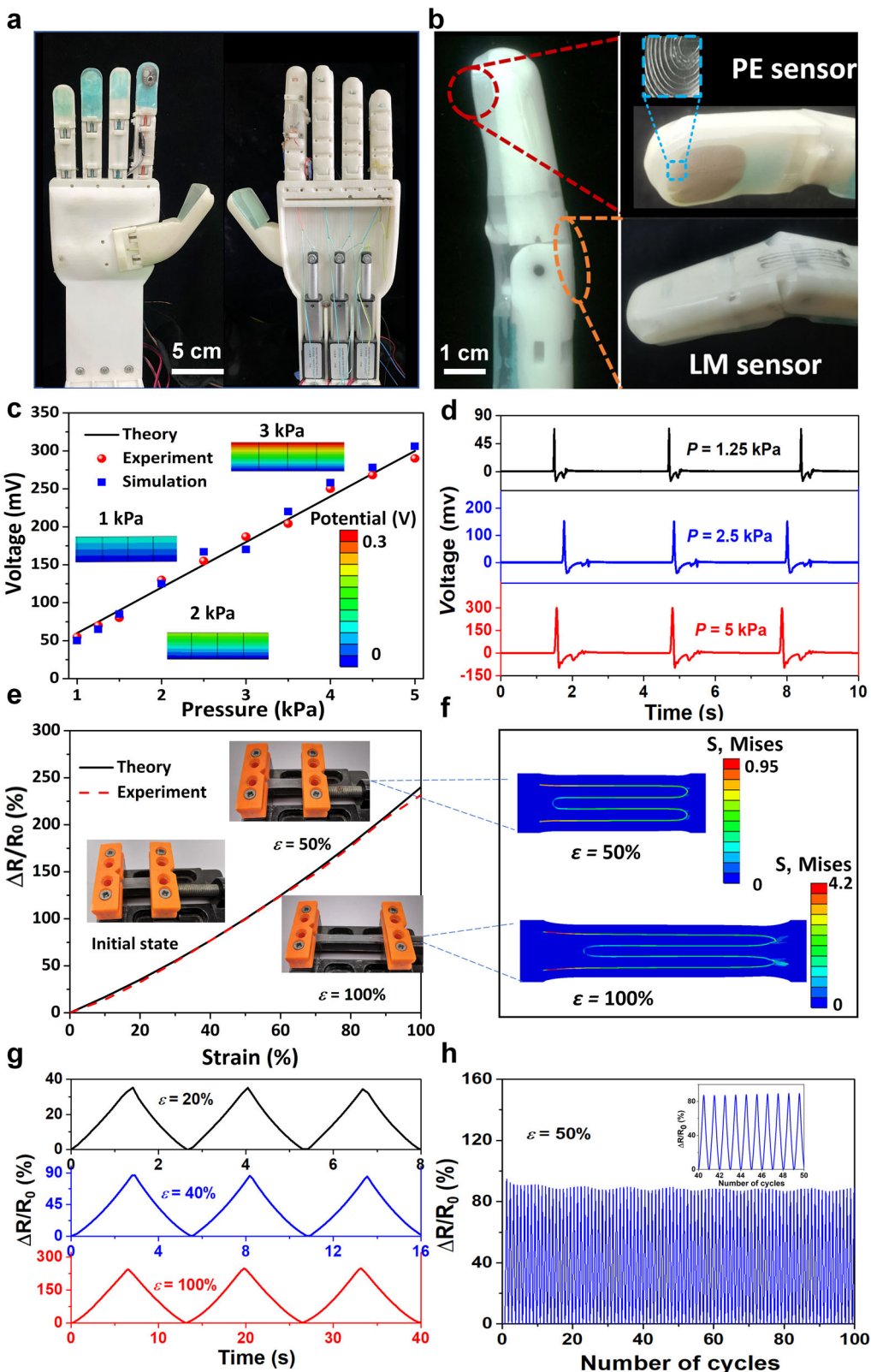


Fig. 2 The sensing performance of the multisensory tactile sensors. **a** Optical images of 3D printed biomimetic manipulator. **b** Optical images of the fabricated integrated sensing system with flexible piezoelectric and strain sensors. **c** A comparison of the piezoelectric voltage between the theoretical predictions, simulation results, and experimental demonstrations as a function of the applied pressure. **d** The voltage output of the flexible piezoelectric layer under various applied pressure as a function of time. **e** A comparison of relative resistance change of LM under applied tensile strain range from 0% to 100% between the theoretical calculation and experimental measurements. **f** Simulation results of stress distributions at top surface of the LM sensor for the applied 50% and 100% tensile strain. **g** Experimental demonstrations of relative resistance change of LM under applied tensile strain range from 20% to 100%. **h** Working stability of the LM sensor tested over 100 cycles under a tensile strain of 50%.

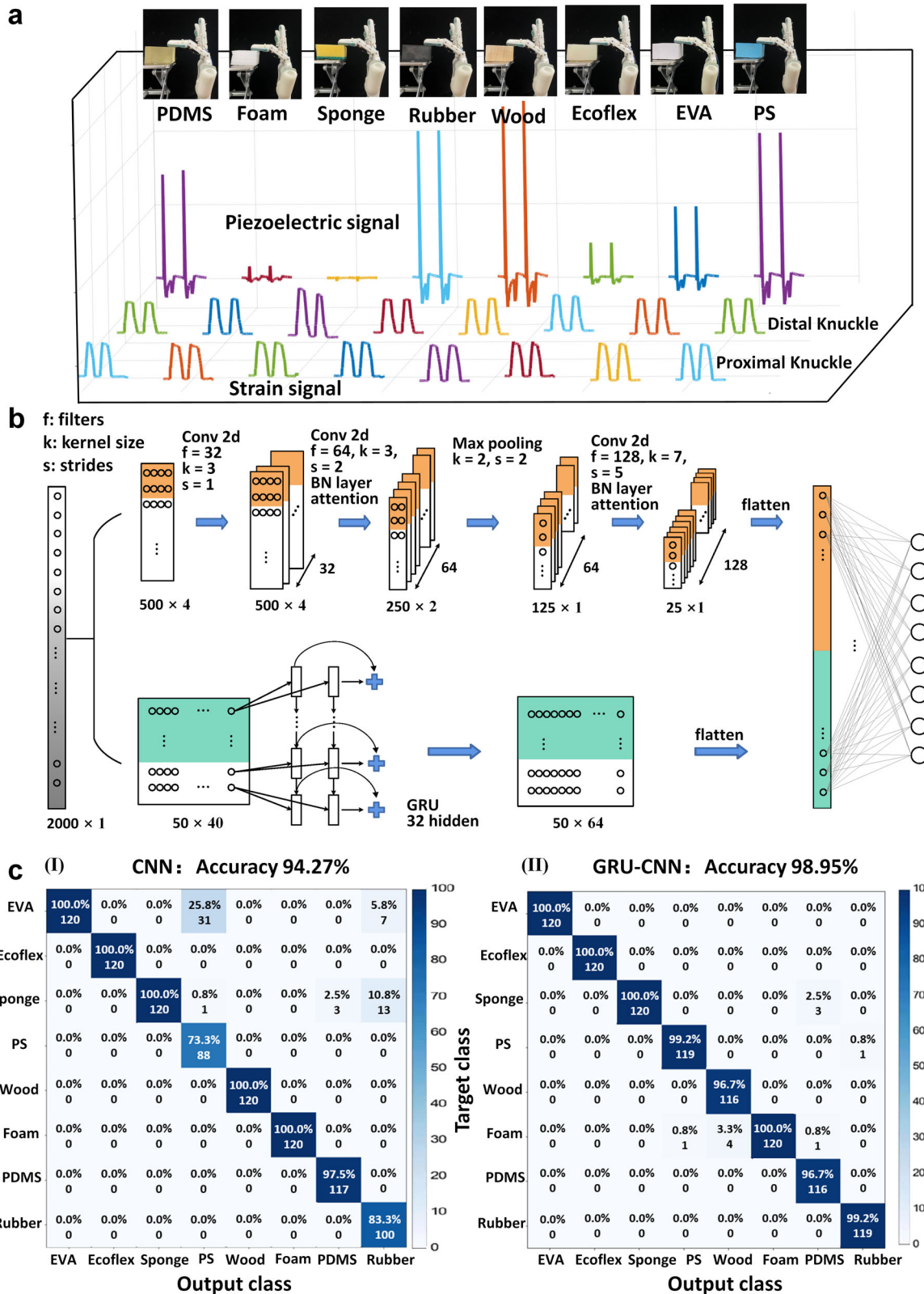


Fig. 3 Multisensory output-based object softness classification utilizing machine learning technique. a Corresponding piezoelectric outputs and relative resistance change from the piezoelectric mode and strain mode in recognizing eight objects. **b** Schematics of the process and parameters for constructing the GRU-CNN. **c** Classification test confusion matrix of object recognition derived from the piezoelectric sensing signal through two models made by (I) CNN and (II) GRU-CNN.

fluoride-trifluoroethylene, P(VDF-TrFE)) and strain (liquid alloy, EGaIn) sensors as multifunctional somatosensory receptors (Fig. 2b). The piezoelectric sensor integrated in the fingertip is designed to facilitate the acquisition of dynamic signals when the robot touches an object. Meanwhile, the piezoresistive strain sensors integrated in the proximal and distal finger ends to obtain the bending information are designed through positive kinematic analysis calculations (Supplementary Figs. 5 and 6). In particular, the fingertip molds are 3D printed based on the principle of Fused Deposition Modeling, which depends on the nozzle extruding the material with circular sections and stacking it layer by layer. Gaps between the extrudate during molding lead to the printed mold with fingertip-inspired structures, thus the fingertip skin has a fingerprint-like structure by pouring PDMS in the mold and demolding. Thus, the fingerprint-inspired structure (Supplementary Fig. 7) on the fingertip skin is adopted to enhance adhesion and friction, thereby improving the strain with surface deformation.

The sensing mechanism and performance of the dual-mode sensors can be evaluated quantitatively through theoretical/numerical analysis and experimental measurement tools (Fig. 2c). The piezoelectric sensing mechanism lies in the reorientation of the aligned molecular dipoles within the piezoelectric layer while the dynamically changing pressure is applied. The relations between the piezoelectric voltage and pressure of the piezoelectric module can be further predicted by an electro-mechanical analytical model³⁶. Results show well-behaved, linear variations of piezoelectric voltage with respect to applied pressure. To further validate the theoretical calculation, finite element analysis (FEA) is performed using ABAQUS software via the continuum element C3D8E to study the piezoelectric potential of the piezoelectric film. The experimental sensing performance of the piezoelectric film is investigated by measuring the voltage output upon the application of mechanical pressure (Fig. 2d). The experimental result shows that the piezoelectric voltage increases rapidly as the pressure increases from 1.25 kPa to 5 kPa with a sensitivity of 60 mV/kPa, which agrees reasonably well with results from finite element analyses and theoretical calculation. Evaluation of the piezoelectric sensor (Supplementary Fig. 8) indicates the minimum detectable pressure is 100 Pa, whereas the maximum detection limit is 12 kPa. The response time of the piezoelectric mode is determined to be 12 ms. The comparison with previously reported sensors in terms of sensitivity, response time, and detection limits (Supplementary Table 1) indicate that piezoelectric sensors in this work are performing well. We further show the measured piezoelectric voltage according to the applied bending strain for 100 cycles (Supplementary Fig. 9), which reveals that the piezoelectric layer has good mechanical stability. In addition, the stability measuring of piezoelectric output is performed, the 14-day measurements demonstrate that the piezoelectric voltage has good stability (Supplementary Fig. 10a). The piezoelectric voltage also remains stable when interacting with different material (e.g., PI, PET, AL) surfaces (Supplementary Fig. 10b).

Detecting the static and low-frequency mechanical stimuli is also crucial for the electronic sensor to mimic the sensory capability of the human skin. The stretchable strain sensors integrated at finger joints are designed and fabricated using patterned LM wires based on the gallium-based alloy (Ga: In 75:25 wt %). The capability of capturing static pressure relies on a continuous electrical response of active piezoresistive sensing elements. The theoretical relationship between the resistance changes and deformation indicates that the increased strain of LM wire leads to rapidly enhanced resistance, which is further confirmed by the experimental measurement upon the uniaxial tensile strain (Fig. 2e and Supplementary Note 1). The sensitivity of the strain sensor at different strain corresponding gauge factors (GF_s) is also plotted (Supplementary Fig. 11). When the applied

strain was below 100%, the resistance increased in a relatively gentle slope that corresponded to a GF_1 of 2.82. At a higher strain of 100–300%, the GF_2 increased from 2.82 to 5.37. The strain sensor exhibits a sensitivity GF_3 of 8.38 within the strain range of 300–500%. The minimum detectable strain and response time of the strain sensor are 0.05% and 163 ms, respectively. The sensing performance of the LM sensor is compared with the reported representative strain sensors (Supplementary Table 2), which shows a favorable comprehensive performance of this sensing system. To further explore the strain distribution of LM wire during the stretching process, the FEA result of LM modeled as Neo-Hookean hyperelastic material (C3D8H) demonstrates that the stress within serpentine layout distributed LM wires is uniform without sudden concentration (Fig. 2f). For flexible strain sensors, high-mechanical durability under long-time also plays a crucial role in the reliable application. LM sensors show a stretch-and-release performance from 20% to 100% strain loading and unloading cycles with negligible hysteresis (Fig. 2g). However, the sensor has a degree of hysteresis value of 1.3% while the 300% tensile strain is applied (Supplementary Fig. 12), which is attributed to intermolecular forces between the liquid-state conductor and elastomeric substrate and leads to incomplete recovery of the original contact positions. The hysteresis performance compares favorably with some previous literature reported (Supplementary Table 3). Moreover, the sensor has good reversibility and reliability repeated without signal drift or fluctuation after 100 cycles (Fig. 2h).

Qualitative softness classification by machine learning

To validate the reliability for softness measurement of the multifunctional sensing system, the integrated sensory modules comprise two sensing mechanisms (i.e., piezoelectric and strain) to simultaneously detect dynamic and static mechanical stimuli during the recognition process. For the purpose of acquiring adaptive contact-force to achieve scarless grasping, the first step of softness differentiation relies on a preliminary classification of the eight standard samples having different Young's moduli (i.e., sponge, foam, Ecoflex, Polydimethylsiloxane [PDMS], Ethylene Vinyl Acetate [EVA], Polystyrene, rubber, and wood). The manipulator gently touches various measured samples with the same contact force and speed each time, which leads to a synchronous response of piezoelectric and strain sensing signals. The principal component analysis method is further performed on multimodal signals to extract the main features and reduce the dimension of effective information. The recognition accuracy of two sensing signals is compared with that of a single piezoelectric signal (Supplementary Fig. 13), which shows the recognition accuracy of the above two cases (i.e., 94.78% and 94.27%) are quite close. Moreover, it consumes more time and computational resources due to the increase in databases. The measured peak value of piezoelectric voltage varies obviously with the types of objects (Fig. 3a), indicating that the piezoelectric signal plays a crucial role in detecting dynamic stimuli and is suitable for providing sensory feedback to classify the softness.

Incorporating neural networks and deep learning with sensing systems to create robotic perception and recognition are an effective approach for classification^{65,66}. A two-stream convolutional network (gate recurrent unit [GRU]- convolutional neural network [CNN]) is designed to effectively acquire the spatial-temporal features of original complex signals (Fig. 3b), which is attributed to the synergistic effect of two neural networks. Furthermore, all algorithms in this work are implemented in TensorFlow. In particular, eight types of objects with various softness are touched by a manipulator, and each object has thirty groups of sensing signals. The collected 240 sets of data were randomly disordered, of which 60% were used as training data for the network and 40% as test data. The sensing signals are

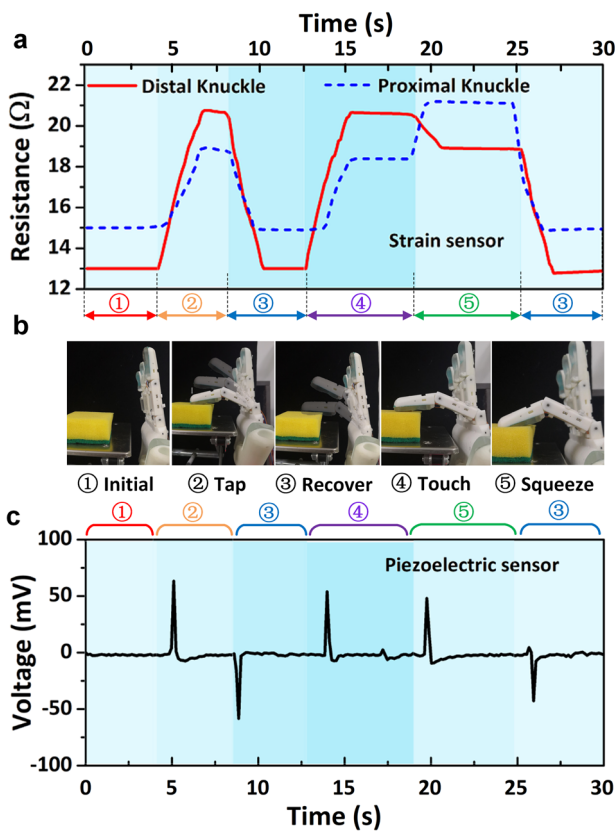


Fig. 4 The sensing demonstrations of the multisensory tactile sensors during the softness recognition procedure. a Measured relative resistance change of LM sensors integrated in the proximal and distal finger ends of a manipulator. **b** Optical images of the manipulator movement in the process of identifying the softness of the sponge. **c** The voltage output of the flexible piezoelectric layer as a function of time while the manipulator touches the sponge.

converted into instantaneous image signals by 2D convolution for processing. The CNN utilizes a sliding convolution kernel to extract the peak value variation of the piezoelectric signal. Meanwhile, the GRU is adopted to acquire the strong sequential correlation characteristics between piezoelectric signals. The confusion map of models in Fig. 3c shows that the CNN method is capable of assisting the manipulator to achieve above 94.27% accuracy of softness recognition (Fig. 3c-i), whereas features learned from the GRU-CNN model further improve the recognition accuracy to 98.95% even with limited training data (Fig. 3c-ii). The comparable results indicate that the collaboration of two kinds of deep neural networks can increase the training efficiency and improve the interaction of features, resulting in an enhancement of recognition accuracy.

With the aid of the piezoelectric signal and deep learning, eight types of standard samples are distinguished and classified into four softness categories (i.e., A, B, C, D). According to the preliminary classification results, various contact forces are applied to the standard samples of different softness categories for the subsequent second step of quantitative softness discrimination. The adaptive contact force is exerted to obtain the relative resistance change from the strain mode to further quantify softness, which prevents permanent damage to objects from excessive pressing. The measuring mechanism lies in the theory of contact mechanics that takes into account the elastic deformation of the object due to contact forces (Supplementary Note 2), determining the essential softness performance evaluated through the elastic coefficient. The measurement in static

principle calculates the elastic coefficient based on the sample deformation measured by the strain sensor and the deformation of the fingertip piezoelectric sensor acquired from force-displacement curves (Supplementary Fig. 14).

Working mechanism of softness identification

Verifying the reliability for softness measurement of samples is crucial to adapting the proposed testing method to practical scenarios. The whole measurement is illustrated through an identification of the elastic coefficient of sponge, as an example, is shown in Fig. 4. In particular, it is feasible to divide the recognition process into two steps: (i) qualitative softness classification perceived by the piezoelectric mode and (ii) quantitative detection measured by the strain mode. Representative movements of manipulator during the period of the preliminary judgment include touching and releasing. When the biomimetic finger touches the sponge, the piezoelectric voltage of 65 mV is generated due to an action of the dynamic stimulus. Combining the piezoelectric output and machine learning technique, the measured results indicate that the softness classification of sponge belongs to A category.

Relying on the appropriate contact force of 2.5 N from the classification results, the subsequent quantitative recognition gestures of the manipulator consisting of touching and squeezing the sponge are performed. The change of finger joint angles leads to an increase in the relative resistance change of the strain sensor at the proximal and distal finger ends (Fig. 4a), which is utilized to detect the deformation of the measured objects. Meanwhile, the deformation of the skin on the fingertip made of PDMS is obtained from the force-displacement curve. The calculation results show that the elastic coefficient and deformation of the sponge are 16.47 N/mm and 2.09 mm, respectively, and the elastic coefficient of the sponge is 1.1 N/mm. The softness classification and assigned contact forces of other samples are also explored to obtain the elastic coefficient (Supplementary Table 4). The quantitative testing results agree reasonably well with results from experimental observations, and the average relative error is controlled within 10%. Therefore, the designed measuring strategy utilizes the synergistic effect of piezoelectric and strain modes to decode the softness, providing a quantitative identifying methodology in a non-destructive manner.

With an effective softness identification provided by the multifunctional sensing system, the feedback information is beneficial for the manipulator to regulate the adaptive contact force to execute a grasping movement. To further explore the stable grasping capability of the manipulator integrated with sensing modules, representative four objects (i.e., sponge, Ecoflex, PDMS, and wood) with different softness are used to demonstrate the grasping procedure. The role of the intelligent sensing system on the stable grasping capability of the manipulator has been further confirmed by a direct comparison between with and without sensing modules (Fig. 5a). The experimental observations show that the manipulator without sensing function grasps the object with a fixed contact force, leading to large deformation and damage to the soft sponge (Fig. 5a-I). When grasping heavy objects such as wood blocks, insufficient frictions induced by the small grasping force make the block slide and fail to achieve stable grasping (Fig. 5a-IV). Additional grasping demonstrations are further conducted to extend the capability to capture fragile objects (e.g., soft tofu, mature tomato) in daily life (Fig. 5b), which requires highly sensitive sensing feedback and grasping force adjustment to complete stable grasping action. A comparative result indicates that the manipulator with sensing feedback function is capable of grasping tofu and tomato stably (Fig. 5b-I and II), whereas the manipulator without the sensing modules results in damage to tofu and tomato (Fig. 5b-III and IV). Furthermore, an evaluation of the grasping performance of the

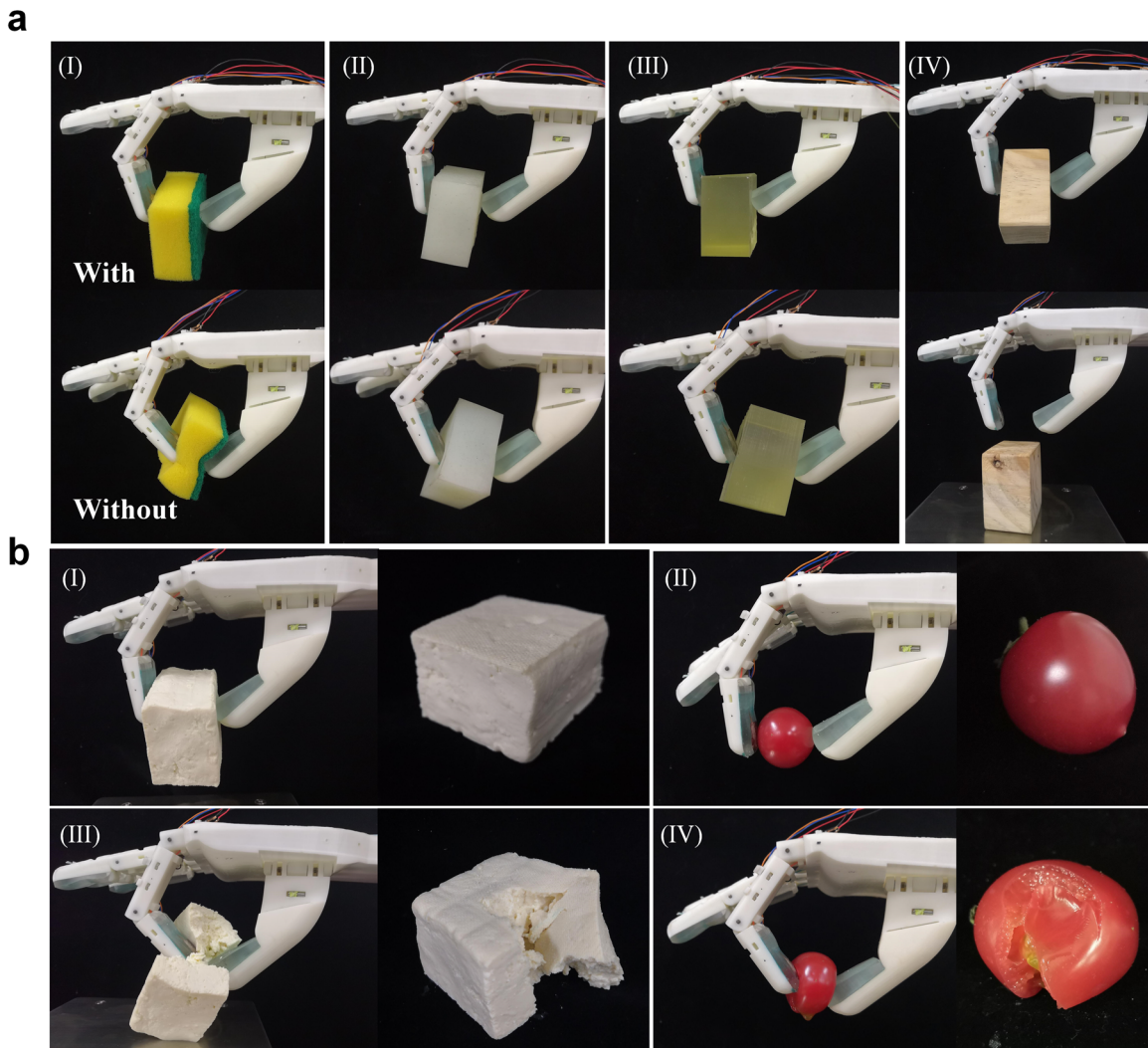


Fig. 5 A comparison of the manipulator with and without sensing modules integration for grasping objects. a Demonstration of grasping four types objects using a manipulator. **b** Demonstration of grasping tofu and tomato using a manipulator.

manipulator with one sensing mode is also performed (Supplementary Fig. 15). The manipulator with a piezoelectric module has voltage feedback when lightly touching the strawberry, which is not sufficient for the subsequent quantitative detection. Meanwhile, a single strain sensing module causes damage to the gripping strawberry due to the inability to obtain a pre-appropriate grasping force. Therefore, the multifunctional sensing system can assist the manipulator to achieve softness identification in a non-invasive manner through sensing feedback and grasping force adjustment.

Applications of flexible sensors on the intelligent sorting

Softness recognizing and adaptive grasping capability of the biomimetic manipulator creates application opportunities for intelligent sorting in smart robots, neural prosthetics, and future human-machine interfaces. To validate the feasibility of the dexterous tasks, the manipulator with multifunctional sensing modules is demonstrated to distinguish and grab delicate oranges on the assembly line toward the intelligent sorting (Fig. 6 and Supplementary Videos 1 and 2). Oranges are vulnerable to damage in the process of industrial picking because of their low elastic modulus and thin epidermis. As a proof-of-concept demonstration, effectively distinguishing the softness of fresh and rotten oranges is highly desired to induce self-regulated and

feedback-type grasping movement (Fig. 6a, c). The measuring results show that the softness of oranges can be recognized by the integrated piezoelectric and strain sensors (Fig. 6b, d). The softness-dependent grasping force regulation is utilized to enable the manipulator integrated in the robot arm to further perform a stable grasping action, which achieves intelligent sorting of oranges with different freshness. The developed multisensory electronic skin that is capable of identifying the softness of touched materials in a non-invasive manner shows potential applications in intelligent robotics, human-machine interfaces, and electronic prostheses. On the basis of this proof of concept, the remaining challenges in the softness recognition of non-homogeneous objects will be addressed through further understanding and optimizing the dual-mode sensing arrays.

DISCUSSION

In summary, we demonstrated an approach utilizing the bioinspired multifunctional sensing systems to quantify the elastic coefficient of soft materials in a non-invasive manner, enabling the biomimetic manipulator to realize adaptive grasping. This identification methodology lies in the preliminary classification of softness by piezoelectric signals and modified machine learning algorithms with 98.95% accuracy, which facilitates the subsequent

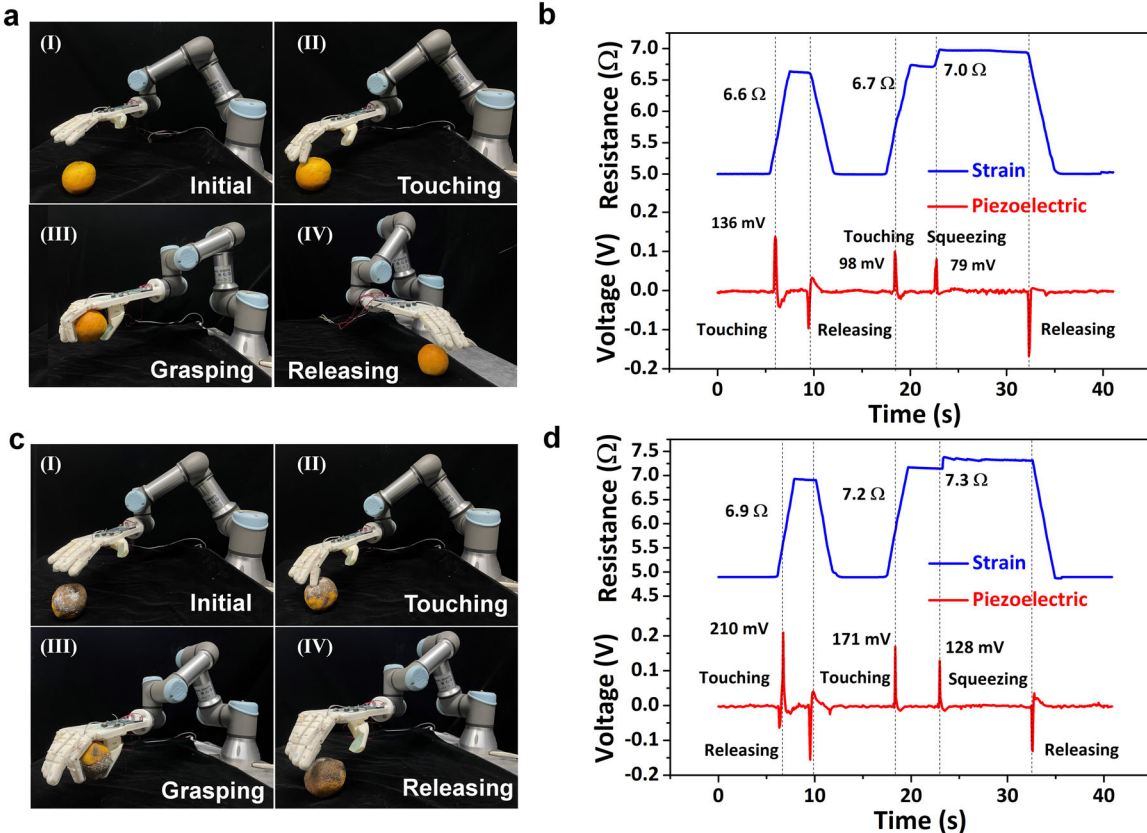


Fig. 6 Integrated demonstration in intelligent sorting applications. Optical images of a manipulator integrated in the robot arm for sorting **a** a fresh and **c** rotten oranges; Measured resistance and voltage output from the strain and piezoelectric sensors during the process of grasping **b** fresh and **d** rotten oranges.

quantitative measurement through strain sensing feedback. Such exhibited synergistic effect of the multifunctional sensing modules allows the manipulator to recognize various soft materials with softness ranging from 30 kPa to 10 MPa, which delivers application opportunities in dexterous grasping tasks of fragile objects (e.g., tomato and tofu). As a proof-of-concept demonstration, the developed biomimetic manipulator with multisensory capabilities and grasping adaptability is successfully integrated into the robot arm to achieve the intelligent sorting of fresh and rotten oranges. This research provides a strategy toward undestroyed softness measurements and would broadly benefit many fields, especially for intelligent soft robotics, minimally invasive surgery, and electronic prostheses.

METHODS

Fabrication of the biomimetic manipulator

The biomimetic manipulator constructed in solidworks software is created and developed using 3D printing technology (Formlab, Form2) to complete the assembly procedure. The control module of the biomimetic manipulator is programmed on the microcontroller Arduino NANO V3 development board with the analog-to-digital conversion module (AD620) and the 12 V power supply (Supplementary Note 3).

Fabrication of P(VDF-TrFE) piezoelectric sensors

0.5 g of P(VDF-TrFE) powder (Piezotech) was first dissolved in 20 ml of N,N-Dimethylformamide and magnetically stirred for 2 hours to obtain a uniform solution. The P(VDF-TrFE) film was prepared by casting the uniform solution on the petri dish and curing in the vacuum oven at 70 °C for 10 hours to remove the solvent. The thermal annealing process was carried out at 120 °C for 2 hours to improve crystallinity, which was confirmed by the Fourier transform infrared spectroscopy measurement

(Supplementary Fig. 16) and relevant analyses²⁴. After peeling off from the petri dish, the piezoelectric film was placed in a silicone oil bath for half an hour at a high electric field of 60 MV·m⁻¹ to be polarized (Supplementary Fig. 17). The polarization setup includes a silicone oil bath and a high voltage power (Supplementary Fig. 18). The thickness of the electrodes must ensure good electrical conductivity while not restricting the deformation of the piezoelectric film. Evaporating the gold electrodes with a thickness of 150 nm on both sides of the piezoelectric film was conducted using an electron beam evaporator (DZS-500). The fabrication of the piezoelectric sensors ended with attaching the copper wires to the upper and lower gold electrodes. The thickness of the prepared piezoelectric sensor is 35 μm. Meanwhile, the area of the piezoelectric sensor is 2 cm². Encapsulating the entire piezoelectric sensor with two polydimethylsiloxanes (PDMS) films on both sides completed the fabrication of the device (Supplementary Fig. 19). PDMS (Sylgard 184, Dow Corning) was prepared by mixing base with crosslinker (10:1 in mass ratio), degassed and spin-coated (300 rpm for 1 min) on the fingertip mold, followed by baking at 60 °C for 20 min. After curing, the piezoelectric sensor was attached to the cured PDMS surface and then covered by another PDMS layer for encapsulation.

Fabrication of LM sensors

The eutectic metal alloy was synthesized by mixing gallium and indium in a 3:1 weight ratio (EGaIn, Sigma-Aldrich), which maintains a liquid state at room temperature (15.7 °C melting point). A homogeneous eutectic metal alloy was achieved after stirring at room temperature with 500 rpm for 2 min and 2000 rpm (vigorously stirred) for 8 min. The LM wire was patterned and fabricated on an Ecoflex (Smooth-On, 00-30) substrate by printing technology (Supplementary Fig. 20). The dimensions of the pattern used for the preparation of the meander structure are 15 mm × 3 mm. The copper wires were then attached to the printed LM wire, another Ecoflex encapsulation layer was coated on the top and cured in the oven at 60 °C for 30 min. The thickness of the encapsulated sensor is 0.3 mm. The length and width dimensions of the sensor are 20 mm ×

- 10 mm. Meanwhile, a single EGaN wire with a wire width of 0.4 mm. The resistivity of the LM material is $29.4 \times 10^{-6} \Omega/\text{cm}$. The fabricated LM sensor can withstand a variety of deformations (Supplementary Fig. 21).
- ## Measurements of the sensing performance of the multifunctional sensing modules
- The piezoelectric property (e.g., $d_{33} = 32 \text{ pC/N}^{-1}$) of the P(VDF-TrFE) film was measured using a quasi-static d_{33} tester (ZJ-6A of the Chinese Academy of Sciences). To characterize the electrical response, the sensing signals from strain and piezoelectric sensors were obtained using a semiconductor parameter analyzer (4200-SCS, Keithley) and piezoelectric data acquisition system (KSI), respectively.
- ## DATA AVAILABILITY
- The data that support the findings of this study are available from the corresponding author upon reasonable request.
- Received: 11 January 2022; Accepted: 31 May 2022;
Published online: 15 June 2022
- ## REFERENCES
- Tian, L. et al. Large-area MRI-compatible epidermal electronic interfaces for prosthetic control and cognitive monitoring. *Nat. Biomed. Eng.* **3**, 194–205 (2019).
 - Chortos, A., Liu, J. & Bao, Z. Pursuing prosthetic electronic skin. *Nat. Mater.* **15**, 937–950 (2016).
 - Delmas, P., Hao, J. & Rodat-Despoix, L. Molecular mechanisms of mechanotransduction in mammalian sensory neurons. *Nat. Rev. Neurosci.* **12**, 139–153 (2011).
 - Lai, Y. et al. Actively perceiving and responsive soft robots enabled by self-powered, highly extensible, and highly sensitive triboelectric proximity- and pressure-sensing skins. *Adv. Mater.* **30**, 1801114 (2018).
 - Wang, Z. et al. Signal filtering enabled by spike voltage-dependent plasticity in metalloporphyrin-based memristors. *Adv. Mater.* **33**, 2104370 (2021).
 - Hartmann, F., Drack, M. & Kaltenbrunner, M. Meant to merge: Fabrication of stretchy electronics for robotics. *Sci. Robot.* **3**, eaat9091 (2018).
 - Wang, C. et al. Soft ultrathin electronics innervated adaptive fully soft robots. *Adv. Mater.* **30**, 1706695 (2018).
 - Lee, Y. et al. Stretchable organic optoelectronic sensorimotor synapse. *Sci. Adv.* **4**, eaat3787 (2018).
 - Kim, J. et al. Stretchable silicon nanoribbon electronics for skin prosthesis. *Nat. Commun.* **5**, 5747 (2014).
 - Yang, Y. et al. A laser-engraved wearable sensor for sensitive detection of uric acid and tyrosine in sweat. *Nat. Biotechnol.* **38**, 217–224 (2020).
 - Wang, Y. et al. All-weather, natural silent speech recognition via machine-learning-assisted tattoo-like electronics. *npj Flex. Electron.* **5**, 20 (2021).
 - Kaltenbrunner, M. et al. An ultra-lightweight design for imperceptible plastic electronics. *Nature* **499**, 458–463 (2013).
 - Ning, X. et al. Mechanically active materials in three-dimensional mesostructures. *Sci. Adv.* **4**, eaat8313 (2018).
 - He, K. et al. An artificial somatic reflex arc. *Adv. Mater.* **32**, 1905399 (2020).
 - Wang, R. et al. Tensile and torsional elastomer fiber artificial muscle by entropic elasticity with thermo-piezoresistive sensing of strain and rotation by a single electric signal. *Mater. Horiz.* **7**, 3305–3315 (2020).
 - Ha, M. et al. Reconfigurable magnetic origami actuators with on-board sensing for guided assembly. *Adv. Mater.* **33**, 2008751 (2021).
 - Parida, K., Bhavanasi, V., Kumar, V., Bendi, R. & Lee, P. Self-powered pressure sensor for ultra-wide range pressure detection. *Nano Res.* **10**, 3557–3570 (2017).
 - Jang, K. et al. Soft network composite materials with deterministic and bio-inspired designs. *Nat. Commun.* **6**, 6566 (2015).
 - Shi, C. et al. Heterogeneous integration of rigid, soft, and liquid materials for self-healable, recyclable, and reconfigurable wearable electronics. *Sci. Adv.* **6**, eabd0202 (2020).
 - Ha, T. et al. A chest-laminated ultrathin and stretchable e-tattoo for the measurement of electrocardiogram, seismocardiogram, and cardiac time intervals. *Adv. Sci.* **6**, 1900290 (2019).
 - Wang, C. et al. Programmable and scalable transfer printing with high reliability and efficiency for flexible inorganic electronics. *Sci. Adv.* **6**, eabb2393 (2020).
 - Zhou, H. et al. Stretchable piezoelectric energy harvesters and self-powered sensors for wearable and implantable devices. *Biosens. Bioelectron.* **168**, 112569 (2020).
 - Zhang, Y. et al. Climbing-inspired twining electrodes using shape memory for peripheral nerve stimulation and recording. *Sci. Adv.* **5**, eaaw1066 (2019).
 - Zhang, C. et al. 3D printed, solid-state conductive ionoelastomer as a generic building block for tactile applications. *Adv. Mater.* **34**, e2105996 (2021).
 - Qiu, Y. et al. Bioinspired, multifunctional dual-mode pressure sensors as electronic skin for decoding complex loading processes and human motions. *Nano Energy* **78**, 105337 (2020).
 - Liu, Z. et al. An ultrasensitive contact lens sensor based on self-assembly graphene for continuous intraocular pressure monitoring. *Adv. Funct. Mater.* **31**, 2010991 (2021).
 - Zhai, Z., Wang, Y., Lin, K., Wu, L. & Jiang, H. In situ stiffness manipulation using elegant curved origami. *Sci. Adv.* **6**, eabe2000 (2020).
 - Wang, C. et al. Stretchable, multifunctional epidermal sensor patch for surface electromyography and strain measurements. *Adv. Intell. Syst.* **3**, 2100031 (2021).
 - Han, X. et al. Flexible polymer transducers for dynamic recognizing physiological signals. *Adv. Funct. Mater.* **26**, 3640–3648 (2016).
 - Wang, F. et al. Flexible doppler ultrasound device for the monitoring of blood flow velocity. *Sci. Adv.* **7**, eabi9283 (2021).
 - Qu, C. et al. Bioinspired flexible volatile organic compounds sensor based on dynamic surface wrinkling with dual-signal response. *Small* **15**, e1900216 (2019).
 - Su, Y., Dagdeviren, C. & Li, R. Measured output voltages of piezoelectric devices depend on the resistance of voltmeter. *Adv. Funct. Mater.* **25**, 5320–5325 (2015).
 - Qiu, Y. et al. A biomimetic drosera capensis with adaptive decision-predation behavior based on multifunctional sensing and fast actuating capability. *Adv. Funct. Mater.* **32**, 2110296 (2022).
 - Jin, Y. et al. Identifying human body states by using a flexible integrated sensor. *npj Flex. Electron.* **4**, 28 (2020).
 - Wang, Q. et al. Self-healable multifunctional electronic tattoos based on silk and graphene. *Adv. Funct. Mater.* **29**, 1808695 (2019).
 - Qiu, Y. et al. The frequency-response behaviour of flexible piezoelectric devices for detecting the magnitude and loading rate of stimuli. *J. Mater. Chem. C* **9**, 584–594 (2021).
 - Bai, N. et al. Graded intrafillable architecture-based iontronic pressure sensor with ultra-broad-range high sensitivity. *Nat. Commun.* **11**, 209 (2020).
 - Wang, X. et al. Somatosensory, light-driven, thin-film robots capable of integrated perception and motility. *Adv. Mater.* **32**, 2000351 (2020).
 - Cheng, L. et al. A highly sensitive piezoresistive sensor with interlocked graphene microarrays for meticulous monitoring of human motions. *J. Mater. Chem. C* **8**, 11525–11531 (2020).
 - Li, S. et al. Contact-resistance-free stretchable strain sensors with high repeatability and linearity. *ACS Nano* **16**, 541–553 (2022).
 - Zhao, Y. et al. Somatosensory actuator based on stretchable conductive photo-thermally responsive hydrogel. *Sci. Robot.* **6**, eabd5483 (2021).
 - Li, D., Yang, S., Chen, X., Lai, W. & Huang, W. 3D Wearable fabric-based micro-supercapacitors with ultra-high areal capacitance. *Adv. Funct. Mater.* **31**, 2107484 (2021).
 - Zhu, M. et al. Haptic-feedback smart glove as a creative human-machine interface (HMI) for virtual/augmented reality applications. *Sci. Adv.* **6**, eaaz8693 (2020).
 - Dhong, C. et al. Role of indentation depth and contact area on human perception of softness for haptic interfaces. *Sci. Adv.* **5**, eaaw8845 (2019).
 - Saal, H., Delhaye, B., Rayhaun, B. & Bensmaia, S. Simulating tactile signals from the whole hand with millisecond precision. *Proc. Natl. Acad. Sci. USA* **114**, E5693–E5702 (2017).
 - Wang, Y. et al. Hierarchically patterned self-powered sensors for multifunctional tactile sensing. *Sci. Adv.* **6**, eabb9083 (2020).
 - Ma, X. et al. Sensor embedded soft fingertip for precise manipulation and softness recognition. *IEEE Robot. Autom. Lett.* **6**, 8734–8741 (2021).
 - Pang, K. et al. Hydroplastic foaming of graphene aerogels and artificially intelligent tactile sensors. *Sci. Adv.* **6**, eabd4045 (2020).
 - Sundaram, S. et al. Learning the signatures of the human grasp using a scalable tactile glove. *Nature* **569**, 698–702 (2019).
 - Chun, S. et al. Self-powered pressure- and vibration-sensitive tactile sensors for learning technique-based neural finger skin. *Nano Lett.* **19**, 3305–3312 (2019).
 - Lu, H., Hong, Y., Yang, Y., Yang, Z. & Shen, Y. Battery-less soft millirobot that can move, sense, and communicate remotely by coupling the magnetic and piezoelectric effects. *Adv. Sci.* **7**, 2000069 (2020).
 - Yu, X. et al. Needle-shaped ultrathin piezoelectric microsystem for guided tissue targeting via mechanical sensing. *Nat. Biomed. Eng.* **2**, 165–172 (2018).
 - Kim, K. et al. Tactile avatar: tactile sensing system mimicking human tactile cognition. *Adv. Sci.* **8**, 2002362 (2021).
 - Yan, Y. et al. Soft magnetic skin for super-resolution tactile sensing with force self-decoupling. *Sci. Robot.* **6**, eabc8801 (2021).
 - Cui, Z. et al. Haptically quantifying young's modulus of soft materials using a self-locked stretchable strain sensor. *Adv. Mater.* e2104078 (2021).

56. Song, E. et al. Miniaturized electromechanical devices for the characterization of the biomechanics of deep tissue. *Nat. Biomed. Eng.* **5**, 759–771 (2021).
57. Beker, L. et al. A bioinspired stretchable membrane-based compliance sensor. *Proc. Natl Acad. Sci. USA* **117**, 11314–11320 (2020).
58. Lee, G. et al. Fingerpad-inspired multimodal electronic skin for material discrimination and texture recognition. *Adv. Sci.* **8**, 2002606 (2021).
59. Li, G., Liu, S., Wang, L. & Zhu, R. Skin-inspired quadruple tactile sensors integrated on a robot hand enable object recognition. *Sci. Robot.* **5**, eabc8134 (2020).
60. Sengupta, D., Romano, J. & Kottapalli, A. G. P. Electrospun bundled carbon nanofibers for skin-inspired tactile sensing, proprioception and gesture tracking applications. *npj Flex. Electron.* **5**, 29 (2021).
61. Johansson, R. & Flanagan, J. Coding and use of tactile signals from the fingertips in object manipulation tasks. *Nat. Rev. Neurosci.* **10**, 345–359 (2009).
62. Park, J., Kim, M., Lee, Y., Lee, H. & Ko, H. Fingertip skin-inspired microstructured ferroelectric skins discriminate static/dynamic pressure and temperature stimuli. *Sci. Adv.* **1**, e1500661 (2015).
63. Boutry, C. et al. A hierarchically patterned, bioinspired e-skin able to detect the direction of applied pressure for robotics. *Sci. Robot.* **3**, eaau6914 (2018).
64. Chun, K., Son, Y., Jeon, E., Lee, S. & Han, C. A self-powered sensor mimicking slow- and fast-adapting cutaneous mechanoreceptors. *Adv. Mater.* **30**, 1706299 (2018).
65. Zhang, Z. et al. Deep learning-enabled triboelectric smart socks for IoT-based gait analysis and VR applications. *npj Flex. Electron.* **4**, 29 (2020).
66. Mahler, J. et al. Learning ambidextrous robot grasping policies. *Sci. Robot.* **4**, eaau4984 (2019).

ACKNOWLEDGEMENTS

This work was supported by National Natural Science Foundation of China (Grant no. 11672269, 11972323, and 12002308); Zhejiang Provincial Natural Science Foundation of China (Grant no. LQ22A020009, LR20A020002, LR18E050002, LR19E020004, LZY21E030002, D21F030003, and LSY19H180004); Fundamental Research Funds for the Provincial Universities of Zhejiang (RF-B2019004); 111 Project (No.: D16004); Department of Education of Zhejiang Province (Y202043208).

AUTHOR CONTRIBUTIONS

Y.Q., and S.S. conceived the idea and planned the experiments. K.S. and Z.W. performed the experiments and helped in the realization of sensor. X.M., G.B., X.W.,

and W.Z. wrote the control programs and algorithms for demonstration. Y.T., Z.Z., H. C., A.L., and H.W. contributed to the data analysis. Y.Q. wrote the paper. All authors discussed the results and commented on the manuscript.

COMPETING INTERESTS

The authors declare no competing interests.

ADDITIONAL INFORMATION

Supplementary information The online version contains supplementary material available at <https://doi.org/10.1038/s41528-022-00181-9>.

Correspondence and requests for materials should be addressed to Huaping Wu.

Reprints and permission information is available at <http://www.nature.com/reprints>

Publisher's note Springer Nature remains neutral with regard to jurisdictional claims in published maps and institutional affiliations.



Open Access This article is licensed under a Creative Commons Attribution 4.0 International License, which permits use, sharing, adaptation, distribution and reproduction in any medium or format, as long as you give appropriate credit to the original author(s) and the source, provide a link to the Creative Commons license, and indicate if changes were made. The images or other third party material in this article are included in the article's Creative Commons license, unless indicated otherwise in a credit line to the material. If material is not included in the article's Creative Commons license and your intended use is not permitted by statutory regulation or exceeds the permitted use, you will need to obtain permission directly from the copyright holder. To view a copy of this license, visit <http://creativecommons.org/licenses/by/4.0/>.

© The Author(s) 2022